

# Split and Knit: 3D Fingerprint Capture with a Single Camera

Apoorva Srivastava

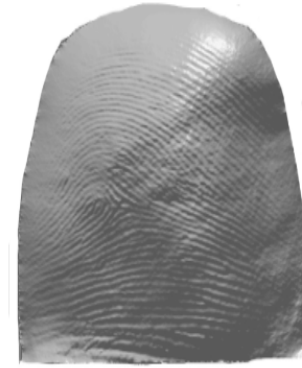
Biometrics and Secure ID Lab, CVIT, IIIT Hyderabad  
India

Anoop M. Namboodiri

Biometrics and Secure ID Lab, CVIT, IIIT Hyderabad  
India



Finger Image



Photometric Stereo based 3D  
Phalange Point Cloud assuming  
finger surface to be Lambertian



3D Phalange Point Cloud  
obtained using Split and Knit  
Algorithm

Figure 1: The proposed Split and Knit (SnK) algorithm produces a more detailed 3D finger phalange point cloud compared to existing photometric stereo-based algorithms that assume the finger surface to be lambertian. SnK takes into account the non-lambertian nature of the finger skin and modifies the captured image to get a superior quality 3D point cloud.

## ABSTRACT

3D fingerprint capture is less sensitive to skin moisture levels and avoids skin deformation, which is common in contact-based sensors, in addition to capturing depth information. Unfortunately, its adoption is limited due to high cost and system complexity. Photometric stereo provides an opportunity to build low-cost, simple sensors capable of high-quality 3D capture. However, it assumes that the surface being imaged is lambertian (unlike our fingers).

We introduce the Split and Knit algorithm (SnK), a 3D reconstruction pipeline based on the photometric stereo for finger surfaces. It introduces an efficient way of estimating the direct illumination component, thus allowing us to do a higher-quality reconstruction of the entire finger surface. The algorithm also introduces a novel method to obtain the overall finger shape under NIR illumination, all using a single camera. Finally, we combine the overall finger shape and the ridge-valley point cloud to obtain a 3D finger phalange. The high-quality 3D reconstruction also results in better matching accuracy of the captured fingerprints.<sup>1</sup>

<sup>1</sup>For further details, please visit the project page: <https://apoovasrivastav.github.io/Split-and-Knit-3D-Fingerprint-Capture-with-a-Single-Camera/>

Permission to make digital or hard copies of all or part of this work for personal or classroom use is granted without fee provided that copies are not made or distributed for profit or commercial advantage and that copies bear this notice and the full citation on the first page. Copyrights for components of this work owned by others than the author(s) must be honored. Abstracting with credit is permitted. To copy otherwise, or republish, to post on servers or to redistribute to lists, requires prior specific permission and/or a fee. Request permissions from permissions@acm.org.

ICVGIP'22, December 8–10, 2022, Gandhinagar, India

© 2022 Copyright held by the owner/author(s). Publication rights licensed to ACM.  
ACM ISBN 978-1-4503-9822-0/22/12...\$15.00  
<https://doi.org/10.1145/3571600.3571618>

## CCS CONCEPTS

- Computing methodologies → Computer vision; 3D imaging.

## KEYWORDS

3D Fingerprint Reconstruction, Photometric Stereo

## ACM Reference Format:

Apoorva Srivastava and Anoop M. Namboodiri. 2022. Split and Knit: 3D Fingerprint Capture with a Single Camera. In *Proceedings of the Thirteenth Indian Conference on Computer Vision, Graphics and Image Processing (ICVGIP'22)*, December 8–10, 2022, Gandhinagar, India. ACM, New York, NY, USA, 9 pages. <https://doi.org/10.1145/3571600.3571618>

## 1 INTRODUCTION

Fingerprints are the oldest and most popular form of biometrics. The 2D fingerprint pattern has a very high amount of information to recognize every human being uniquely [16]. Modern AFIS (Automatic Fingerprint Identification Systems) have become an integral part of security systems all across the globe due to their accuracy and ease of use. The primary challenge of such systems is the poor quality of certain fingerprints obtained during the capture process. The capture requires the finger to be pressed against a surface leading to non-uniform skin deformation and inaccurate results. Moreover, the moisture level of the skin and latent prints left on the sensor also plays a key role in the quality of capture. Being a contact-based method, it also raises questions on hygiene and sensor reliability over time.

The 3D fingerprint system has a contactless acquisition of the finger alleviating the above problems. It also provides additional

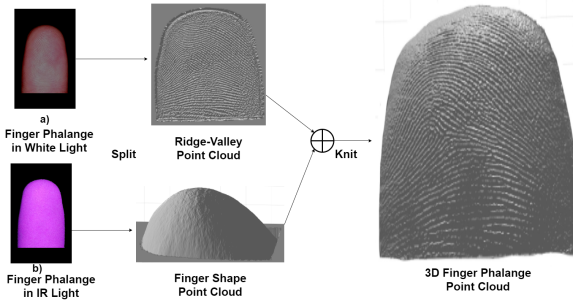


**Figure 2: The SnK algorithm uses a single camera and multiple LEDs to reconstruct a detailed finger phalange point cloud.** a) The visible spectrum image is transformed into a lambertian image using a trained U-Net to obtain the ridge-valley point cloud using photometric stereo. b) NIR(Near-Infrared) images obtained with the same camera are used for the finger shape. The proposed algorithm thus splits the finger information into two parts: the lambertian component of the visible spectrum and the NIR spectrum image, containing the ridge-valley pattern and the overall finger shape, respectively. c) The algorithm then knits together the recovered 2.5D images to obtain the complete 3D finger phalange shape.

depth information lost in the 2D fingerprints. Despite these advantages, 3D fingerprint scanners are not very popular due to their higher cost and complexity.

Among the several approaches to 3D fingerprint capture, photometric stereo provides the lowest cost and system complexity as it can work with a single fixed camera and multiple light sources [22]. Other 3D reconstruction methods use multiple cameras, structured light projectors, or precisely moving parts. As mentioned in Table 2.1 of [8], photometric stereo also provides the highest quality 3D reconstruction. It is possible because of the implicit correspondence in the sequence images captured for photometric stereo. Hence, to design a portable, low-cost 3D fingerprint setup, we choose Photometric Stereo as a suitable 3D reconstruction technique.

Despite these advantages, photometric stereo has a significant drawback. It assumes that the imaged surface is lambertian, reflecting the incident light equally in all directions [22]. Moreover, as photometric stereo can capture very high-frequency patterns, it is susceptible to slight illumination changes leading to high-frequency illumination noise. Unfortunately, the finger surface is non-lambertian and exhibits sub-surface scattering and specular reflection. Still, the current sensors based on photometric stereo assume the finger surface to be lambertian. As this assumption is invalid, these solutions restrict their reconstruction to a patch of the finger, ignoring its overall shape.

The Split-and-Knit algorithm (*SnK*) is a 3D reconstruction pipeline based on the photometric stereo for the finger surface. The two properties of the finger surface that lead to its non-lambertian nature are i) Sub-surface scattering and ii) Specular reflection. The basic philosophy of the algorithm, to overcome the drawbacks of the non-lambertian surface, lies in reconstructing the finger as the sum of a high-frequency ridge-valley pattern and low-frequency

finger shape. The algorithm separates the reconstruction of the high and low-frequency patterns by observing the finger in visible and near-infrared (NIR) light, respectively.

For reconstructing the ridge-valley point cloud for the whole finger surface, we reduce sub-surface scattering using a novel U-Net model and specific image processing steps to remove specularity and low-frequency information. Utilizing a novel way of observing the finger in NIR light, we instantly eliminate the specular reflection, sub-surface scattering, and high-frequency information to obtain the finger shape. We also introduce another novel way to obtain finger shapes without NIR illumination using reflective surfaces and parametric modeling. Finally, we combine the ridge-valley point cloud and the finger shape to obtain the 3D finger phalange model. The existing photometric stereo-based reconstruction can be considered the baseline for our work. We improve the baseline for finger surfaces using the SnK algorithm. Figure 2 explains the Split-and-Knit(*SnK*) algorithm in a nutshell.

The main contributions of our work are:

- 1) A solution that extracts the ridge-valley pattern from the finger and re-mix it with the finger shape to obtain the 3D finger phalange with detailed fingerprint information and accurate overall shape, all using a single camera (for the first time to our knowledge).
- 2) A method for global-direct component separation, using a trained U-Net without extra hardware, which reduces the non-lambertian nature of the finger image and provides a detailed ridge-valley pattern.
- 3) A method to capture the overall finger shape using the same camera via two novel approaches a) using NIR illumination and b) using a parametric model for the finger shape from a reflective surface without NIR illumination.

## 1.1 Related Works

**Photometric Stereo based systems:** The work by Kumar *et al.* [9] is most closely related to our work. They pioneered the use of photometric stereo for 3D fingerprint reconstruction. They mixed 3D and 2D fingerprint minutiae matching scores to give the highest possible accuracy for 3D fingerprints. The only limitation of their work is that they assumed the finger surface to be lambertian; hence, they could obtain the 3D fingerprint only for a finger patch without proper finger shape. Also, the matching results were not good when they used only 3D features. Further, Zheng *et al.* [28] obtained even higher matching accuracy for 3D fingerprints using minutiae obtained from surface normals and albedo. They also assumed the finger surface to be lambertian. In the follow-up work by C.Lin *et al.* [12], they improved the 3D matching accuracy by using colored LEDs to detect and correct finger motion. Their work focused on improving the accuracy and speed of the 3D minutiae matching algorithm using a tetrahedron-based matching approach. They also mixed the 2D and 3D fingerprint features to obtain their best results. All the above methods focussed on improving the finger matching accuracy instead of improving the 3D fingerprint reconstruction quality. All of them assumed the finger surface to be lambertian and used the same method of the reconstruction as mentioned by Kumar *et al.* in [9]. Hence, we consider [9] as the baseline for our work. Xie *et al.* [24] proposed an HK model for modeling finger surfaces to decrease the effect of the sub-surface scattering

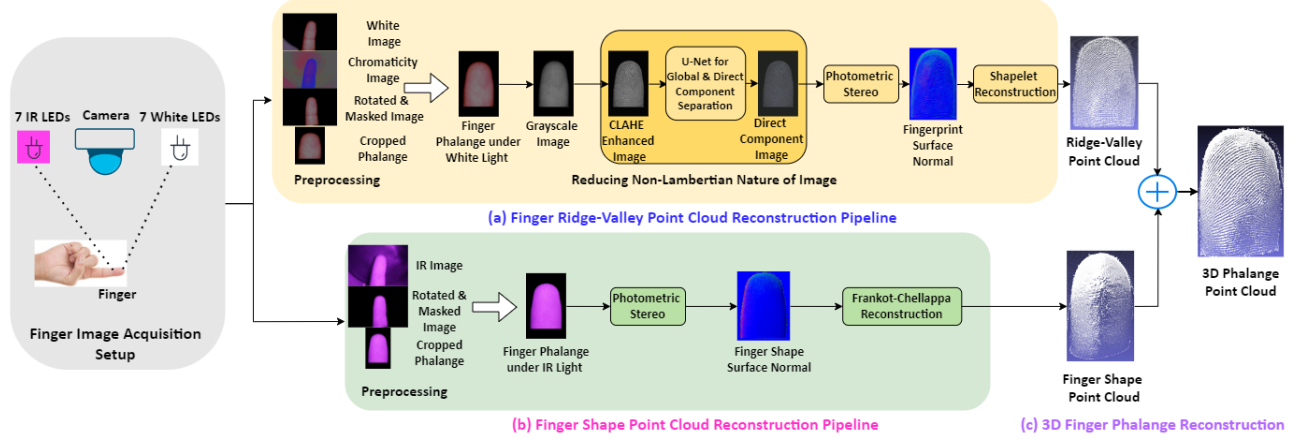


**Figure 3: The Split-and-Knit Algorithm(SnK) consists of three primary components:** (a) Reconstruction pipeline for finger ridge-valley point cloud. The white light images are preprocessed to obtain cropped phalange. Using CLAHE [18] and global-direct component separation by U-Net, the non-lambertian nature of the finger image is reduced. Further, using photometric stereo and shapelet reconstruction [7], finger ridge-valley point cloud is obtained (b) Reconstruction pipeline for finger shape point cloud. The NIR light images are preprocessed to obtain cropped phalange. Further, we apply photometric stereo and Frankot-Chellappa reconstruction [3] to obtain the finger shape point cloud. (c) The phalange point cloud is obtained by pixel-wise addition of the ridge-valley and finger shape point cloud.

property of the finger. It is the only work based on the photometric stereo that focuses on addressing the non-lambertian nature of the finger and improving the 3D reconstruction quality. However, the results obtained were not significantly different from the lambertian finger model, as mentioned in figure 3.18 of [8].

**Other Approaches:** Stereo Vision-based methods involve using bulky and complex setups having two or more cameras to obtain fingerprint images from multiple viewpoints. Among the multiple views, they find correspondences to get good quality 3D fingerprints [2, 13, 14, 17]. However, the primary issue with stereo vision-based methods is finding the correspondences. The correspondences are found for the blocks of the pixels rather than the pixels themselves. It leads to less accurate fingerprint reconstructions as block correspondences make the 3D reconstruction noisy.

In Structured-Lighting-based systems, multiple pattern-shifted images are projected and captured. The correspondences are established based on the projected pattern, which is more reliable than the stereo vision method. In methods proposed in [5, 10, 21, 25, 27], the advantage is that they can recover ridge-valley details and achieve relatively accurate 3D depth information along with a smooth overall shape. However, the hardware system of these methods is expensive and bulky. Also, the increase in projection and capture frequency requires a more sophisticated projector and camera.

Other methods like Optical Coherence Tomography [1, 20] and LASER-based methods [4] to obtain the 3D finger point cloud, but both of these methods have bulky and non-portable systems. Hence, all these methods do not suit the portable 3D fingerprint setup.

**Methods for Obtaining Finger Shape:** The finger shape can be easily obtained using structured light and stereo vision methods as they are independent of the optical properties of the surface. Yan

*et al.* [26] used six cameras to create a visual hull of the finger to obtain a 3D finger shape, vein model, and finger texture. Labati *et al.* [11] provided a simulation method for synthesizing fingertips based on 2 virtual views. However, to the best of our knowledge, it is the first time we have obtained the finger shape using a single camera and photometric stereo.

**Organization of the Paper:** Section 2 details the Split-and-Knit (SnK) algorithm. Each sub-section highlights the components of the algorithm: ridge-valley reconstruction, finger-shape reconstruction, and integration of the two to obtain finger phalange. Section 3 discusses the experiments and analysis, followed by conclusions and future works in section 4.

## 2 SPLIT-AND-KNIT ALGORITHM:

### 2.1 Overview

The Split-and-Knit algorithm(SnK) aims to obtain 3D finger phalange using a single camera and photometric stereo. It is challenging as photometric stereo requires the surface to be lambertian and is also sensitive to high-frequency illumination noise. In contrast, the finger surface is non-lambertian and exhibits sub-surface scattering and specular reflection. The non-lambertian nature of the finger poses two challenges: *i*) It prevents the capture of ridge-valley point cloud for the whole finger area.*ii*) It distorts the overall finger shape. To deal with the above challenges, the Split-and-Knit(SnK) algorithm divides the 3D phalange reconstruction into *three components*:

- 1) Reconstruction of the ridge-valley point cloud,
- 2) Reconstruction of finger shape point cloud,
- 3) Mixing the ridge-valley and finger shape to obtain 3D finger phalange.

Figure 3 details the Split-and-Knit(SnK) algorithm.

## 2.2 Theory

The Photometric Stereo relates the pixel intensities with the surface orientation of an object via a reflectance map [22]. The surface orientation can be expressed in terms of surface gradients. Hence the pixel intensity can be related to the reflectance function using equation 1.

$$I = R(p, q) \quad (1)$$

where p and q are surface gradients in the x and y directions, R is the surface reflectance function, and I is the image pixel intensity at a given point P. Under the orthographic projection of the scene with the viewing axis aligned to the z-axis, an object's surface can be expressed with the values of its z coordinate at a given spatial location x, y i.e.

$$z = f(x, y) \quad (2)$$

The Split and Knit observes the finger surface (z) as the sum of the finger ridge-valley pattern ( $z_1$ ) and the finger shape ( $z_2$ ).

$$z = z_1 + z_2 = f_1(x, y) + f_2(x, y) \quad (3)$$

$$\nabla z = \nabla(f_1(x, y) + f_2(x, y)) \quad (4)$$

Therefore, from equations 1 and 4

$$I = R(\nabla(f_1(x, y)) + \nabla(f_2(x, y))) \quad (5)$$

As  $f_1(x, y)$  and  $f_2(x, y)$  are unknown, they also contain noise due to sub-surface scattering and specular reflection. Hence, we can't calculate them directly as we have single-valued intensity at each point. To calculate them, we segregate the pixel intensity for  $f_1(x, y)$  and  $f_2(x, y)$  through computational illumination by observing fingers in visible and IR light. We use visible light to calculate  $f_1(x, y)$ , the 3D ridge-valley surface.

$$I_{White} = R(\nabla(f_1(x, y)) + \nabla(f_2(x, y))) + \Psi \quad (6)$$

Here  $I_{White}$  is composed of radiance from the ridge valley, finger shape, and noise due to sub-surface scattering and specular reflection represented by  $\Psi$ . We remove the sub-surface scattering effect by extracting the direct component and obtaining the 3D reconstruction. Further, we extract the high-frequency element from the reconstructed finger using Shapelet reconstruction to remove the specular reflection and the low-frequency shape component from equation 6. We observe the finger in NIR light to obtain  $f_2(x, y)$ .

$$I_{NIR} = R(\nabla(f_2(x, y))) \quad (7)$$

The NIR light provides a homogenous appearance to the finger; hence it removes high-frequency ridge-valley from equation 5, and sub-surface scattering and specular reflection do not occur. We can directly reconstruct the finger shape using photometric stereo and Frankot-Chellappa reconstruction.

## 2.3 Reconstruction of 3D Ridge-Valley point cloud

**2.3.1 Overview.** The Split-and-Knit(*SnK*) algorithm obtains the finger ridge-valley point cloud in four steps:

- (1) Pre-Processing of the finger image
- (2) Reducing the non-lambertian nature of the finger image
- (3) Obtaining fingerprint surface normals using photometric stereo

- (4) Ridge-valley point cloud reconstruction from the finger surface normals.

The sub-sections below elaborate upon the steps for obtaining the finger ridge-valley point cloud, shown in Figure 3 (a).

**2.3.2 Pre-Processing.** The pre-processing steps aim to obtain the first phalange segmented at a zero-degree yaw angle for all the finger images. It ensures uniformity in the 3D finger phalange output irrespective of the orientation, size, and skin complexion. The details of the pre-processing steps can be found in the supplementary.

**2.3.3 Reducing the non-Lambertian nature of the finger image.** We performed CLAHE enhancement [18] followed by Global-Direct component separation to reduce the non-lambertian nature of the finger image.

**CLAHE Enhancement:** Contactless fingerprint images have relatively low contrast between ridges and valleys compared with contact fingerprint images. The enhancement step has to be chosen so that it does not entirely distort the lighting direction information stored as pixel intensities. In this regard, we chose adaptive histogram equalization to enhance the contrast based on neighborhood pixel information. However, adaptive histogram equalization amplifies the noise in the homogenous region [18]. To fix this, we applied Contrast Limited Adaptive Histogram Equalization (CLAHE), which clips the slope of the transformation function, thus preventing the noise amplification [18]. We applied CLAHE over the 64x64 neighborhood window of the grayscale fingerprint images.

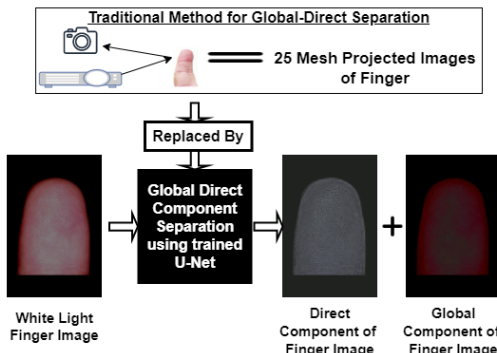


**Figure 4: To reduce the non-lambertian nature of the finger image, we need the Direct component of the finger image. Traditionally, the Global-Direct Separation is done using 25 mesh images captured with the help of a camera and projector [15]. We replaced the hardware setup with a trained U-Net to provide the Direct component of the finger image. The Global component is obtained by subtracting the Direct component from the visible spectrum finger image.**

### Global-Direct component separation using trained U-Net:

When a source of light illuminates a scene, the radiance of each point in the scene has two components, namely, direct and global. The direct component of the radiance is due to the source's direct illumination of the surface point, depicting surface geometry. The

global radiance component is due to the illumination of the surface point by interior surface points and scene points, depicting its surrounding composition. Nayar *et al.* [15] separated the global-direct component of a scene using computational illumination. The finger surface exhibits translucent subsurface scattering, a global illumination component emitting beneath the finger surface. For a good 3D reconstruction, we require the image's direct component and the global component's removal. Following the checkerboard method mentioned in [15], we separated the global-direct components for 50 palm images. The palm images are considered because the skin on the palm and fingers are the same, so we get to separate the direct component of the same skin. Also, capturing a palm image will provide more pixels for direct global separation and hence more data for training the U-Net. We took 25 images with the shifted checkerboard pattern of each palm surface. The direct image is obtained as follows:

$$L_{direct} = L_{max} - L_{min} \quad (8)$$

where,  $L_{direct}$  is the direct image of the palm surface,  $L_{max}$  and  $L_{min}$  are the maximum and the minimum image out of 25 checkerboard images of a single palm. We extracted 750 patches of size  $72 \times 72 \times 3$  from every image, leading to 37,500 direct image patches.

Capturing 25 images under shifted checkerboard patterns for direct component separation while fingerprint capture is not feasible. Note that for using photometric stereo, we will need a set of 25 images for each direction of illumination. It increases the acquisition time and requires extra hardware. Our solution is to train an image-to-image neural network to separate the direct component of an image. Jacobson *et al.* [6] have trained an Encoder-Decoder-based neural network to separate the direct component. As our image domain was limited to palm images, we trained a U-Net [19], specifically for separating the direct component of the palm surface. We chose U-Net because it can preserve global and local details of the image, which is crucial for the fingerprint image. We can experiment with the variations of the U-Net to get better results. But, as we got satisfactory results with the basic U-Net, we continued with the basic U-Net for simplicity. Upon restricting the scene to the images of palms, we model the direct component segregation problem as a machine-learning problem for a specific pattern and surface. We used the direct image patch dataset created using the checkerboard method. The depth of the encoder-decoder stage of U-Net is kept at three to reduce its complexity. We replace the segmentation layer of the U-Net with the regression layer of mean squared error loss to generate the direct component of the finger images. Figure 4 shows the finger's direct and global image. The global component is obtained by subtracting the direct component from the image.

**2.3.4 Photometric Stereo for obtaining surface normals of fingerprint.** We apply the photometric stereo on the direct image of the fingers obtained in the previous step. Photometric Stereo is a technique that relates the radiance value recorded in an image to the object's surface geometry via a reflectance map [22].

$$I = R(p, q) \quad (9)$$

For a diffused lambertian model, the reflectance function can be written as

$$R(p, q) = k \cdot \cos i \quad (10)$$

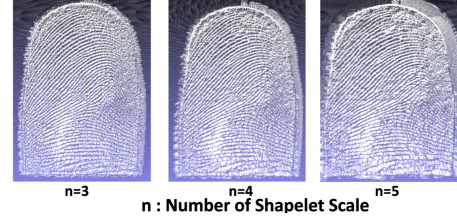


Figure 5: With an increase in the number of shapelet scale( $n$ ), the low-frequency information increases, which distorts the global finger shape. We found the initial 3 shapelet scales most suitable to extract the ridge-valley point cloud.

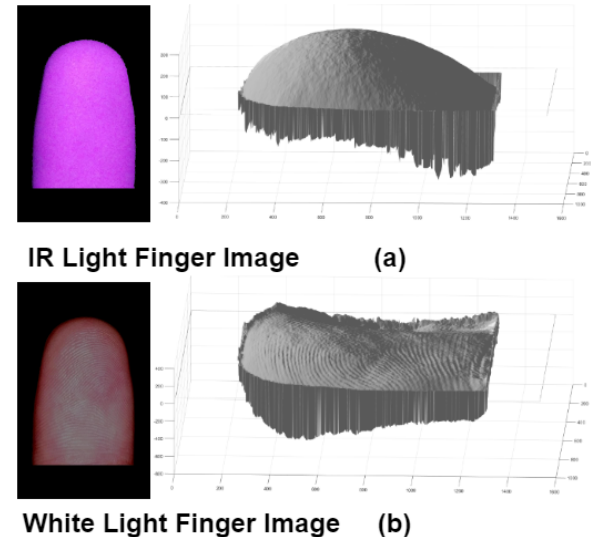


Figure 6: Finger shape obtained using photometric stereo under (a) NIR light illumination, (b) White light illumination. Distortion in shape under the white light is due to the non-lambertian nature of the finger surface.

where  $k$  is the surface constant known as albedo,  $i$  is the incident angle between the surface normal and the illumination direction [22].

$$I = k \cdot N \cdot L \quad (11)$$

where,  $I$  is the pixel intensity,  $N$  is the unit surface normal, and  $L$  is the unit vector of the illumination direction at point P. To determine the value of unit surface normal, we need at least three observations of point P in different illumination directions. However, following [9], we took seven images in different illumination directions to minimize noise. Photometric Stereo is for reconstructing static scenes. Hence, we create a support for the finger to restrict the finger's movement during the capture. The finger is kept on the support and held with the other hand.

**2.3.5 Obtaining Point Cloud of finger ridge-valley using Shapelet Reconstruction.** The Shapelet Reconstruction method converts the surface normals into the 3D point cloud. In the previous step, the algorithm reduces the sub-surface scattering of the finger

image by applying CLAHE enhancement and separating the direct component of the finger image. It helps in obtaining the fingerprint of the entire finger surface. However, the reconstructed 3D structure has the specular reflection noise and the low-frequency shape component, as given by equation 6. So, shapelet reconstruction extracts the ridge-valley pattern from the distorted finger structure. Shapelets are the non-orthogonal redundant set of basis functions whose gradients are correlated with the surface gradients, and correlations are summed to obtain the surface [7]. The size of the shapelet scales decreases with the number of shapelets. As the shapelet decreases in size, its frequency increases. Figure 5 shows that as the shapelet scale increases from  $n = 3$  to  $n = 5$ , there is an increase in low-frequency shape information, distorting the overall finger shape. A detailed analysis of the Shapelet Scale variation is present in the supplementary material. We chose  $n=3$  as the suitable shapelet scale based on the analysis.

## 2.4 Reconstruction of 3D finger shape

As we discussed, the photometric stereo is best suited for high-frequency surface geometry and is susceptible to the slightest illumination noise in pixel values, specifically specular reflection. The finger shape is low-frequency information that gets distorted due to specular reflection and applied image processing to reduce the lambertian nature of the finger image in the previous step. So we reconstruct the shape separately. We propose two novel approaches for finger shape reconstruction using the same camera that is used to capture the ridge-valley pattern: (i) The first approach utilizes two facts about the finger imaging process: a) Most camera sensors are also capable of capturing images in the Near IR (NIR) spectrum, and b) under NIR illumination the high-frequency ridge-valley structures are not visible, revealing the overall finger shape. (ii) The second approach uses one mirror placed on the side of the finger, providing a side elevation image of the finger in the same camera. Please refer to the supplementary material for details of the mirror-based approach for finger shape reconstruction.

**2.4.1 Reconstruction of finger shape using a single camera under NIR illumination:** We observe the finger in NIR illumination to obtain the overall finger shape separately. The same camera can be used to observe visible and NIR spectra. The finger skin consists of three layers, Epidermis, Dermis, and Subcutaneous tissue layer. The white light suffers sub-surface scattering and specular reflection due to the epidermis and dermis layers of the skin. The NIR rays penetrate deeper into the skin to the subcutaneous layer and are absorbed by the water, and fat tissue in this layer [23]. It leads to the removal of sub-surface scattering and specular reflection coming from the epidermis and dermis layers. Also, the ridge-valley structure resides in the epidermis layer, which is not visible in NIR illumination; hence we filter out the high-frequency information using the computational illumination method. The finger surface appears homogeneous under NIR illumination. This homogeneous appearance reveals the undistorted overall shape as depicted by equation 7. Figure 6 compares the shape of the finger obtained under white light and the NIR light using photometric stereo.

## 2.5 Mixing the fingerprint and finger shape to obtain 3D finger phalange

We obtain the ridge-valley point cloud and finger shape point cloud separately. These represent the higher and lower frequency bands of the finger's range image. The 3D finger phalange is obtained by pixel-wise addition of the range image of the fingerprint and the finger shape. It removes the medium frequency spatial noise, which causes finger shape distortion. Figure 3 c) shows the finger phalange reconstructed via the pixel-wise addition of the fingerprint and the finger shape range images.

## 3 EXPERIMENTS AND ANALYSIS

### 3.1 Implementation Details

**3.1.1 Data Collection:** We designed a photometric stereo setup with a Raspberry pi camera, white light, and NIR light LEDs for data collection. The setup was designed to block the external lights as photometric stereo is sensitive to external illumination. The details of the setup can be found in the supplementary material. Data Collection was done over four sessions on different days to match the real-world scenario. Ten fingers of seventeen individuals were collected in four sessions totaling 680 fingers. We discarded some fingers with the roll angle mismatch, where the portion of the finger occluded in one session becomes visible in the other session leading to poor matching results.

**3.1.2 Choice of feature for matching the 3D fingers:** We use LBP (Local Binary Patterns) features obtained from the normal image and the range image of the finger phalange to match the surface normals and 3D point cloud of the finger surface, respectively. Galbally *et al.* [4] also used this feature to compare the depth information in the reconstructed 3D finger point clouds. Although the minutiae matching algorithms are well-established and the most accurate fingerprint-matching techniques, they only match minutiae points. They do not match every point. We chose LBP features instead of minutiae matching as we needed to match every reconstructed 3D point to analyze the quality of fingerprint reconstruction.

### 3.2 Comparative Analysis

We performed qualitative and quantitative comparative studies to display the improvements in the 3D fingerprint reconstruction by *Split-and-Knit Algorithm (SnK)* over the *Existing Algorithms (EA)* [9] based on the photometric stereo. *We considered the following three cases:*

**EA: Existing Algorithms:** 3D finger phalange obtained from gray images of the finger, assuming the finger to be lambertian. The reconstruction is obtained by photometric stereo and Frankot-Chellappa reconstruction [3].

**PR: Partial Result:** 3D finger phalange obtained after CLAHE enhancement and direct component separation of finger image. It is an intermediate result of SnK before extracting ridge-valley point cloud and overall shape addition. Hence, it has a distorted overall shape but a detailed fingerprint pattern.

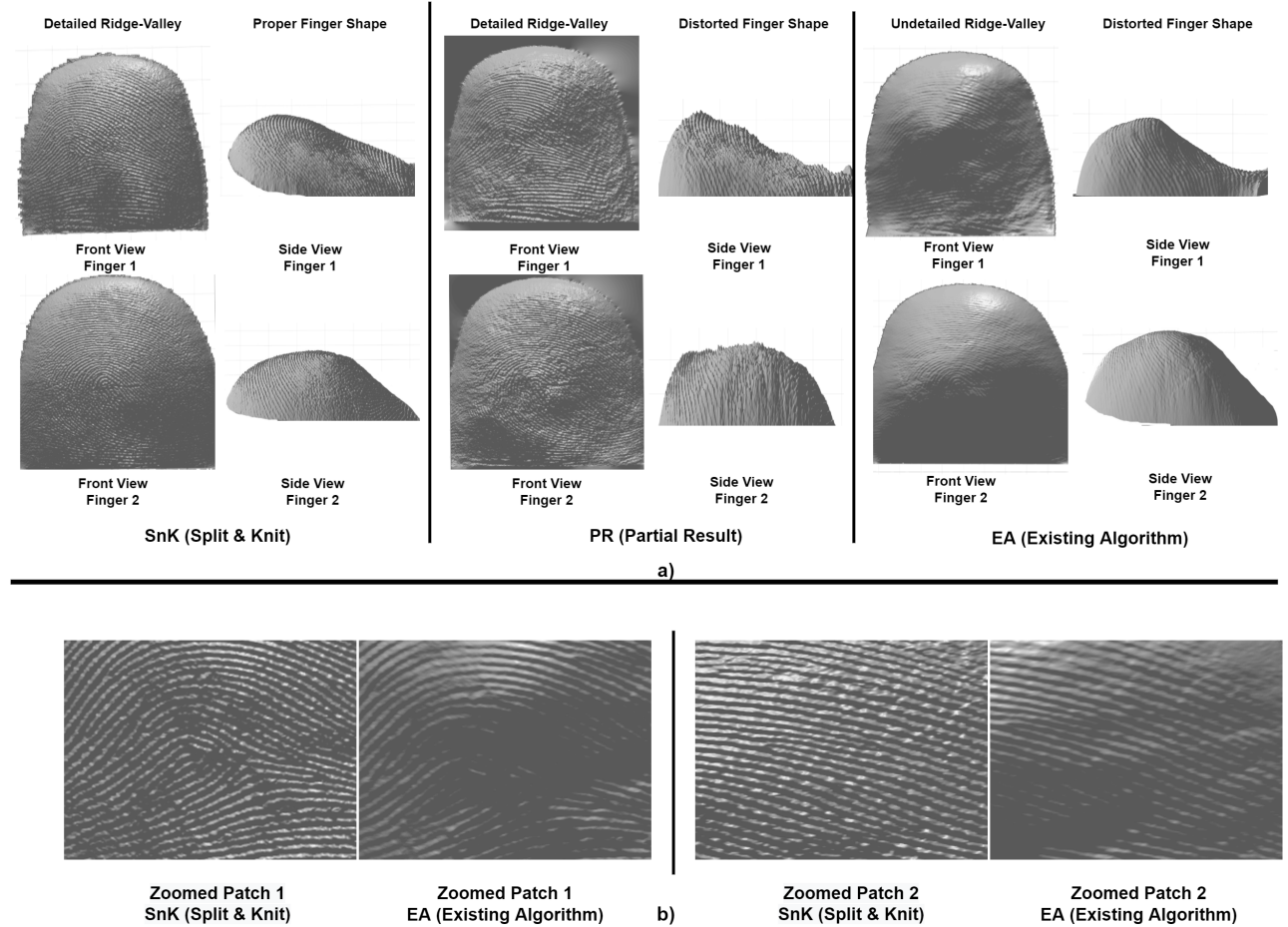


**Figure 7: Qualitative Comparison:** a) Comparison of the front view and side view of the phalange point cloud produced by *SnK*: (*Split-and-Knit*), *PR*: (*Partial Result*), *EA*: (*Existing Algorithm*). The *EA* [9] considers fingers to be lambertian and reconstructs using grayscale images leading to undetailed fingerprints and distorted global shape. The *PR* is the intermediate result obtained after reducing the non-lambertian nature before extracting the ridge-valley and adding global shape leading to a detailed fingerprint but distorted global shape. The *SnK* gives the best result with a detailed fingerprint and proper global shape. b) Comparison of zoomed ridge-valley point cloud for *SnK* and *EA*. *SnK* retrieves superior quality ridge-valley point cloud.

***SnK: Split-and-Knit Algorithm:*** 3D finger phalange obtained after CLAHE enhancement and direct component separation, followed by the addition of extracted ridge-valley point cloud and the finger shape.

**3.2.1 Qualitative Comparison.** Figure 7 shows the qualitative comparison of the 3D point cloud for all three cases: *SnK*, *PR*, *EA*. We conclude the following from Figure 7:

1) The output of *EA*: Existing Algorithms based on the photometric stereo shows its inability to reconstruct the non-lambertian finger surface. It can't capture the fine details of the entire finger surface and the global shape. In comparison, the output of *SnK*: Split-and-Knit algorithm shows the fingerprint of the entire finger surface with the undistorted global shape. The zoomed patches of fingers obtained from *SnK* and *EA* in Figure 7 (b) show the superior quality of the ridge-valley point cloud captured by *SnK* over *EA*.

2) On comparing the *PR* (Partial Results) and the *EA* (Existing Algorithms), the reconstruction for the *PR* captures the finer fingerprint details for the larger finger area. It proves the utility of applying the direct component separation and the CLAHE enhancement.

3) On comparing the *SnK* (Split-and-Knit) and the *PR* (Partial Results), the *PR* reconstruction has the medium frequency noise mixed in shape and the fingerprint, which distorts the finger structure. The improved result of *SnK* over *PR* shows the utility of finger shape addition to the extracted ridge-valley point cloud.

**3.2.2 Quantitative Comparison.** For obtaining the quantitative comparison among the three cases: *SnK* (*Split-and-Knit*), *PR* (*Partial Results*), *EA* (*Existing Algorithm*), we reconstructed and matched 170 fingers captured over 4 sessions using LBP features for each of the three cases. We matched *SnK*, *PR*, and *EA* using surface normals to show the improvement in fingerprint reconstruction quality as

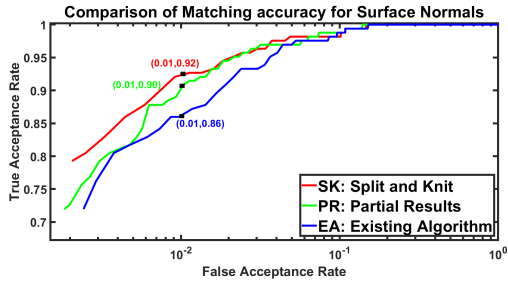


**Figure 8:** ROC curves for matching fingerprint surface normals for *SnK*: Split-and-Knit algorithm, *PR*: Partial Result after reducing the non-lambertian nature of finger image with the distorted overall shape, and *EA*: Existing Algorithms output based on the photometric stereo. The best ROC curve and 92%TAR@0.01FAR are obtained for *SnK*, displaying its highest reconstruction quality.

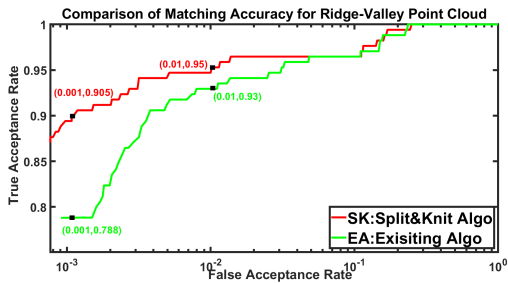


**Figure 9:** ROC curves for matching ridge-valley point cloud obtained from *SnK*: Split-and-Knit algorithm and *EA*: Existing Algorithms based on the photometric stereo. The 95% TAR@0.01 FAR and 90.5% TAR@0.001 FAR of *SnK* as opposed to 93% TAR@0.01 FAR and 78.8% TAR@0.001 FAR of *EA* proves the high quality of the ridge-valley pattern by *SnK*.

shown by the ROCs in Figure 8. We also matched the ridge-valley point cloud obtained for SnK and EA to show the improvement in pattern capture as shown by the ROCs in Figure 9. The Bar-Graph in Figure 10 summarizes the quantitative comparison, which again justifies the conclusions of the qualitative comparison, i.e.

1) The 6% improvement in TAR@0.01 FAR for the surface normal matching of *SnK* as compared to the *EA* displays the better quality reconstruction by SnK, as shown in Figure 8. The 11.7% improvement in TAR@0.001 FAR and 2% improvement in TAR@0.01 FAR for ridge-valley point cloud matching of SnK as compared to EA displays better capturing of the fingerprint details, as shown in Figure 9.

2) The better ROC of surface normal matching of PR over EA in Figure 8 shows detailed pattern capture for PR due to the reduction in the non-lambertian nature of the finger image.

3) The better ROC of surface normal matching of SnK over PR in Figure 8 shows the improvement in the 3D finger due to the addition of the overall finger shape to the ridge-valley point cloud.

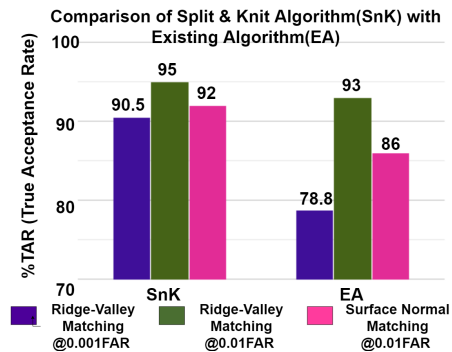


**Figure 10:** The above Bar-Graph compares the matching accuracies of *SnK*: Split-and-Knit algorithm output and *EA*: Existing Algorithms output based on the photometric stereo. The higher % TAR of *SnK* over *EA* for ridge-valley point cloud matching and surface normal matching for all cases show the higher quality of 3D phalange produced by the *SnK*.

## 4 CONCLUSION AND FUTURE WORKS

We presented an algorithm to utilize the photometric stereo for high-quality 3D reconstruction of a finger surface by introducing a novel method to obtain the finger shape using a single camera and mixing it with the extracted ridge-valley point cloud. The qualitative visual comparisons and the matching accuracy improvement using LBP features indicate the better 3D reconstruction quality. However, this is an algorithm to get the 3D fingerprint reconstruction with a single camera. Further experimentation with the capture setup design, camera specifications, and minutiae matching algorithms can help design an end-to-end portable 3D fingerprint recognition system. Apart from the traditional photometric stereo method, deep learning-based photometric methods exist. They apply for non-lambertian surfaces and provide an opportunity for deep learning based 3D fingerprint reconstruction pipelines. Still, they ought to be trained on the fingerprint dataset. Hence, the data produced using the Split and Knit algorithm can be used as ground truth for training such networks. Other possible future research areas are i) Reduction in the computational complexity of the photometric stereo method. ii) Rolled-equivalent fingerprint reconstruction with a single camera to remove roll-angle mismatch in data capture.

## REFERENCES

- [1] Yezeng Cheng and Kirill V. Larin. 2006. Artificial fingerprint recognition by using optical coherence tomography with autocorrelation analysis. *Appl. Opt.* 45, 36 (Dec 2006), 9238–9245. <https://doi.org/10.1364/AO.45.009238>
- [2] Ruggero Donida Labati, Angelo Genovese, Vincenzo Piuri, and Fabio Scotti. 2016. Toward Unconstrained Fingerprint Recognition: A Fully Touchless 3-D System Based on Two Views on the Move. *IEEE Transactions on Systems, Man, and Cybernetics: Systems* 46, 2 (2016), 202–219. <https://doi.org/10.1109/TSMC.2015.2423252>
- [3] R.T. Frankot and R. Chellappa. 1988. A method for enforcing integrability in shape from shading algorithms. *IEEE Transactions on Pattern Analysis and Machine Intelligence* 10, 4 (1988), 439–451. <https://doi.org/10.1109/34.3909>
- [4] Javier Galbally, Laurent Beslay, and Gunnar Böstrom. 2020. 3D-FLARE: A Touchless Full-3D Fingerprint Recognition System Based on Laser Sensing. *IEEE Access* 8 (2020), 145513–145534. <https://doi.org/10.1109/ACCESS.2020.3014796>
- [5] Shujun Huang, Yan Zhao, Jie Dai, Chao Chen, Yongjia Xu, Esther Zhang, and Lili Xie. 2014. 3D fingerprint imaging system based on full-field fringe projection profilometry. *Optics and Lasers in Engineering* 52 (01 2014), 123–130. <https://doi.org/10.1016/j.optlastec.2013.11.010>

- //doi.org/10.1016/j.optlaseng.2013.07.001
- [6] Adam Jacobson, Z. Duan, James C. Bieron, and Pieter Peers. 2020. Deep Separation of Direct and Global Components.
- [7] P. Kovesi. 2005. Shapelets correlated with surface normals produce surfaces. In *Tenth IEEE International Conference on Computer Vision (ICCV'05) Volume 1*, Vol. 2. 994–1001 Vol. 2. <https://doi.org/10.1109/ICCV.2005.224>
- [8] Ajay Kumar. 2018. *Contactless 3D Fingerprint Identification*. Edition 1, Springer Cham.
- [9] Ajay Kumar and Cyril Kwong. 2013. Towards Contactless, Low-Cost and Accurate 3D Fingerprint Identification. In *2013 IEEE Conference on Computer Vision and Pattern Recognition*. 3438–3443. <https://doi.org/10.1109/CVPR.2013.441>
- [10] Ruggiero Donida Labati, Angelo Genovese, Vincenzo Piuri, and Fabio Scotti. 2011. Fast 3-D fingertip reconstruction using a single two-view structured light acquisition. *2011 IEEE Workshop on Biometric Measurements and Systems for Security and Medical Applications (BIOMS)* (2011), 1–8.
- [11] Ruggiero Donida Labati, Angelo Genovese, Vincenzo Piuri, and Fabio Scotti. 2013. Accurate 3D fingerprint virtual environment for biometric technology evaluations and experiment design. *2013 IEEE International Conference on Computational Intelligence and Virtual Environments for Measurement Systems and Applications (CIVEMSA)* (2013), 43–48.
- [12] Chenhao Lin and Ajay Kumar. 2018. Tetrahedron Based Fast 3D Fingerprint Identification Using Colored LEDs Illumination. *IEEE Transactions on Pattern Analysis and Machine Intelligence* 40, 12 (2018), 3022–3033. <https://doi.org/10.1109/TPAMI.2017.2771292>
- [13] Feng Liu and David Zhang. 2014. 3D fingerprint reconstruction system using feature correspondences and prior estimated finger model. *Pattern Recognition* 47, 1 (2014), 178–193. <https://doi.org/10.1016/j.patcog.2013.06.009>
- [14] Feng Liu and David Zhang. 2014. 3D fingerprint reconstruction system using feature correspondences and prior estimated finger model. *Pattern Recognition* 47, 1 (2014), 178–193. <https://doi.org/10.1016/j.patcog.2013.06.009>
- [15] Shree Nayar, Gurumandan Krishnan, Michael Grossberg, and Ramesh Raskar. 2006. Fast separation of direct and global components of a scene using high frequency illumination. *ACM Trans. Graph.* 25 (07 2006), 935–944. <https://doi.org/10.1145/1179352.1141977>
- [16] S. Pankanti, Salil Prabhakar, and Anil Jain. 2002. On the Individuality of Fingerprints. *Pattern Analysis and Machine Intelligence, IEEE Transactions on* 24 (09 2002), 1010–1025. <https://doi.org/10.1109/TPAMI.2002.1023799>
- [17] Geppy Parziale, Eva Diaz-Santana, and Rudolf Hauke. 2006. The Surround Imager™: A Multi-Camera Touchless Device to Acquire 3d Rolled-Equivalent Fingerprints. In *Proceedings of the 2006 International Conference on Advances in Biometrics* (Hong Kong, China) (ICB'06). Springer-Verlag, Berlin, Heidelberg, 244–250. [https://doi.org/10.1007/11608288\\_33](https://doi.org/10.1007/11608288_33)
- [18] Stephen M. Pizer, E. Philip Amburn, John D. Austin, Robert Cromartie, Ari Geselowitz, Trey Greer, Bart Ter Haar Romeny, and John B. Zimmerman. 1987. Adaptive Histogram Equalization and Its Variations. *Comput. Vision Graph. Image Process.* 39, 3 (sep 1987), 355–368. [https://doi.org/10.1016/S0734-189X\(87\)80186-X](https://doi.org/10.1016/S0734-189X(87)80186-X)
- [19] Olaf Ronneberger, Philipp Fischer, and Thomas Brox. 2015. U-Net: Convolutional Networks for Biomedical Image Segmentation. *LNCS* 9351, 234–241. [https://doi.org/10.1007/978-3-319-24574-4\\_28](https://doi.org/10.1007/978-3-319-24574-4_28)
- [20] Ctirad Sousedík, Ralph Breithaupt, and Christoph Busch. 2013. Volumetric finger-print data analysis using Optical Coherence Tomography. In *2013 International Conference of the BIOSIG Special Interest Group (BIOSIG)*. 1–6.
- [21] Yongchang Wang, Laurence G. Hassebrook, and Daniel L. Lau. 2010. Data Acquisition and Processing of 3-D Fingerprints. *IEEE Transactions on Information Forensics and Security* 5, 4 (2010), 750–760. <https://doi.org/10.1109/TIFS.2010.2062177>
- [22] Robert Woodham. 1992. Photometric Method for Determining Surface Orientation from Multiple Images. *Optical Engineering* 19 (01 1992). <https://doi.org/10.1117/12.7972479>
- [23] Shan Xie, Yu Lu, Sook Yoon, Jucheng Yang, and Dong Park. 2015. Intensity Variation Normalization for Finger Vein Recognition Using Guided Filter Based Single Scale Retinex. *Sensors* 15 (07 2015), 17089–17105. <https://doi.org/10.3390/s150717089>
- [24] Wuyuan Xie, Zhan Song, and Xiaoting Zhang. 2010. A Novel Photometric Method for Real-Time 3D Reconstruction of Fingerprint. In *Proceedings of the 6th International Conference on Advances in Visual Computing - Volume Part II* (Las Vegas, NV, USA) (ISVC'10). Springer-Verlag, Berlin, Heidelberg, 31–40.
- [25] VG Yalla and Laurence Hassebrook. 2005. Very high resolution 3-D surface scanning using multi-frequency Phase Measuring Profilometry. *Proceedings of SPIE - The International Society for Optical Engineering* 5798, 44–53. <https://doi.org/10.1117/12.603832>
- [26] Weili Yang, Zhuoming Chen, Junduan Huang, Linfeng Wang, and Wenxiong Kang. 2021. LFMB-3DFB: A Large-scale Finger Multi-Biometric Database and Benchmark for 3D Finger Biometrics. In *2021 IEEE International Joint Conference on Biometrics (IJCB)*. 1–8. <https://doi.org/10.1109/IJCB52358.2021.9484369>
- [27] David Zhang, Guangming Lu, and Lei Zhang. 2018. *3D Fingerprint Reconstruction and Recognition*. Springer International Publishing, Cham, 177–212. [https://doi.org/10.1007/978-3-319-61545-5\\_9](https://doi.org/10.1007/978-3-319-61545-5_9)
- [28] Qian Zheng, Ajay Kumar, and Gang Pan. 2018. Contactless 3D fingerprint identification without 3D reconstruction. *2018 International Workshop on Biometrics and Forensics (IWBF)* (2018), 1–6.